Living cell imaging by far-field fibered interference scanning optical microscopy

Jean-Baptiste Decombe, Wilfrid Schwartz, Catherine Villard, Hervé Guillou, Joël Chevrier, Serge Huant, Jochen Fick

▶ **To cite this version:**

Jean-Baptiste Decombe, Wilfrid Schwartz, Catherine Villard, Hervé Guillou, Joël Chevrier, et al.. Living cell imaging by far-field fibered interference scanning optical microscopy. Optics Express, 2011, 19 (3), pp.2702–2710. 10.1364/OE.19.002702 . hal-00561363

HAL Id: hal-00561363
https://hal.science/hal-00561363

Submitted on 1 Feb 2011

HAL is a multi-disciplinary open access archive for the deposit and dissemination of scientific research documents, whether they are published or not. The documents may come from teaching and research institutions in France or abroad, or from public or private research centers.

L'archive ouverte pluridisciplinaire **HAL**, est destinée au dépôt et à la diffusion de documents scientifiques de niveau recherche, publiés ou non, émanant des établissements d'enseignement et de recherche français ou étrangers, des laboratoires publics ou privés.

Living cell imaging by far-field fibered interference scanning optical microscopy

Jean-Baptiste Decombe, Wilfrid Schwartz, Catherine Villard, Hervé Guillou, Joël Chevrier, Serge Huant, and Jochen Fick*

Institut Néel, CNRS & Université Joseph Fourier, 25 Avenue des Martyrs, BP 166, 38042 Grenoble, France

*jochen.fick@grenoble.cnrs.fr

Abstract: We report on the imaging of biological cells including living neurons by a dedicated fibered interferometric scanning optical microscope. The topography and surface roughness of mouse fibroblasts and hippocampal neurons are clearly revealed. This straightforward far-field technique allows fast, high resolution observation of samples in liquids without lengthy alignment procedures or costly components.

© 2011 Optical Society of America

OCIS codes: (060.2350) Fiber optics imaging; (170.5810) Scanning microscopy; (180.3170) Interference microscopy.

References and links

1. G. Binnig, C. F. Quate, and C. Gerber, "Atomic force microscope," Phys. Rev. Lett. **56**, 930–933 (1986).
2. G. Binnig, H. Rohrer, C. Gerber, and E. Weibel, "Surface studies by scanning tunneling microscopy," Phys. Rev. Lett. **49**, 57–61 (1982).
3. D. W. Pohl, W. Denk, and M. Lanz, "Optical stethoscopy: Image recording with resolution lambda/20," Appl. Phys. Lett. **44**, 651–653 (1984).
4. A. Drezet, A. Hohenau, J. Krenn, M. Brun, and S. Huant, "Surface plasmon mediated near-field imaging and optical addressing in nanoscience," Micron **38**, 427–437 (2007).
5. D. Fotiadis, S. Scheuring, S. A. Müller, A. Engel, and D. J. Müller, "Imaging and manipulation of biological structures with the AFM," Micron **33**, 385–397 (2002).
6. G. Popescu, Y. Park, R. Ramachandra, K. Badizadegan, and M. S. Feld, "Coherence properties of red blood cell membrabe motions," Phys. Rev. E **76**, 031902 (2007).
7. F. Charrière, N. Pavillon, T. Colomb, C. Depeursinge, T. J. Heger, E. A. D. Mitchell, P. Marquet, and B. Rappaz, "Living specimen tomography by digital holographic microscopy: morphometry of testate amoeba," Opt. Express **14**, 7005–7013 (2006).
8. B. Rappaz, F. Charrière, C. Depeursinge, P. J. Magistretti, and P. Marquet, "Simultaneous cell morphometry and refractive index measurement with dual-wavelength digital holographic microscopy and dye-enhanced dispersion of perfusion medium," Opt. Lett. **33**, 744–746 (2008).
9. J. Chevrier, S. Huant, W. Schwartz, and A. Siria, French Patent 08/59091, Université Joseph Fourier - CNRS - CEA (2008), http://www.wipo.int/pctdb/en/wo.jsp?WO=2010076540.
10. R. Stöckle, C. Fokas, V. Deckert, R. Zenobi, B. Sick, B. Hecht, and U. P. Wild, "High-quality near-field optical probes by tube etching," Appl. Phys. Lett. **75**, 160–162 (1999).
11. P. Hoffmann, B. Dutoit, and R.-P. Salathé, "Comparison of mechanically drawn and protection layer chemically etched optical fiber tips," Ultramicroscopy **61**, 165–170 (1995).
12. N. Chevalier, Y. Sonnefraud, J. F. Motte, S. Huant, and K. Karrai, "Aperture-size-controlled optical fiber tips for high-resolution optical microscopy," Rev. Sci. Instr. **77**, 063704 (2006).
13. K. Karrai, G. Kolb, G. Abstreiter, and A. Schmeller, "Optical near-field induced current microscopy," Ultramicroscopy **61**, 299–304 (1995).
14. A. Drezet, J. C. Woehl, and S. Huant, "Diffraction by a small aperture in conical geometry: Application to metal-coated tips used in near-field scanning optical microscopy," Phys. Rev. E **65**, 046611 (2002).
15. A. Drezet, M. J. Nasse, S. Huant, and J. C. Woehl, "The optical near-field of an aperture tip," Europhys. Lett. **66**, 41–47 (2004).

#139255 - $15.00 USD Received 6 Dec 2010; revised 21 Jan 2011; accepted 23 Jan 2011; published 27 Jan 2011
(C) 2011 OSA

16. A. Drezet, A. Cuche, and S. Huant, "Near-field microscopy with a single-photon point-like emitter: Resolution versus the aperture tip," Opt. Commun. **284**, 1444–1450 (2011).
17. O. Brzobohatý, T. Civzmár, and P. Zemánek, "High quality quasi-bessel beam generated by round-tip axicon," Opt. Express **16**, 12688–12700 (2008).
18. W. C. Cheong, B. P. S. Ahluwalia, X.-C. Yuan, L.-S. Zhang, H. Wang, H. B. Niu, and X. Peng, "Fabrication of efficient microaxicon by direct electron-beam lithography for long nondiffracting distance of bessel beams for optical manipulation," Appl. Phys. Lett. **87**, 024104 (2005).
19. H. Guillou, A. Depraz-Depland, E. Planus, B. Vianay, J. Chaussy, A. Grichine, C. Albigès-Rizo, and M. Block, "Lamellipodia nucleation by filopodia depends on integrin occupancy and downstream rac1 signaling," Exp. Cell Res. **314**, 478–488 (2008).
20. B. Vianay, J. Käfer, E. Planus, M. Block, F. Graner, and H. Guillou, "Single cell spreading on a protein lattice adopt an energy minimizing shape," Phys. Rev. Lett. **105**, 128101 (2010).
21. D. Leahy, I. Aukhil, and H. Erickson, "2.0 å crystal structure of a four-domain segment of human fibronectin encompassing the rgd loop and synergy region," Cell **84**, 155–164 (1996).
22. C. Dotti, C. Sullivan, and G. Banker, "The establishment of polarity by hippocampal neurons in culture," J. Neurosci. **8**, 1454–1468 (1988).
23. Y. Nam, D. W. Branch, and B. C. Wheeler, "Epoxy-silane linking of biomolecules is simple and effective for patterning neuronal cultures," Biosens. Bioelectron. **22**, 589–597 (2006).
24. D. F. Bray, J. Bagu, and P. Koegler, "Comparison of hexamethyldisilazane (hmds), peldri ii, and critical-point drying methods for scanning electron microscopy of biological specimens," Microsc. Res. Tech. **26**, 489–495 (1993).
25. L. Abad, M. Petit, G. Bugnicourt, T. Crozes, T. Fournier, and C. Villard, "Neurofets : Field effect nano-transistors fabrication for neural recording," In: Stett A (ed). Proceedings MEA Meeting 2010. Stuttgart: BIOPRO Baden-Württemberg GmbH 2010; 342-343 (2010).
26. G. Kim, "A mechanical spike accompanies the action potential in mammalian nerve terminals," Biophys. J. **92**, 3122–3129 (2007).

1. Introduction

The fast progress in nanosciences experienced over the last decades was made possible thanks to the development of sub-micron resolution, scanning visualization techniques such as Atomic Force Microscopy (AFM) [1], Scanning Tunneling Microscopy (STM) [2], or Near-field Scanning Optical Microscopy (NSOM) [3, 4]. In the field of biology, the AFM is nowadays widely used. However, routine observation of biological cells in water requires dedicated instruments [5]. Phase contrast microscopy is also widely used in biology. It allows noncontact and fast observation of cells. Its resolution is, however, limited by the Rayleigh criterion. Two-and-a-half dimensional quantitative observation was made possible with methods such as the Hilbert Phase Microscope [6] or the Digital Holographic Microscope [7, 8].

In this paper, we present imaging of biological cells by a fibered high-resolution optical microscope, which we call interferometric Scanning Optical Microscope (iSOM) [9]. The topography and surface structure of mouse fibroblasts and living hippocampal neurons are clearly revealed by iSOM. Its working principle is based on the interference of the internally reflected light at an optical fiber tip with the light reflected by the surface facing the tip.

iSOM is complementary to the afore mentioned techniques. It is working in the optical far field, i.e. at tip-sample distances of the order of a few microns. Samples with topography in the micron range can thus be imaged without any mechanical contact, which is of particular importance for the observation of living cells. Moreover, closed-loop tracking of the fiber tip height, as done in AFM or NSOM, is not required. This important feature allows less complex electronic control units to be used at much faster recording speeds. The achieveable resolution is typically half the wavelength laterally to the fiber tip and better than 10 nm axially for highly reflective samples.

iSOM can be developed at reduced costs and is well suited for integration with other measurement techniques, as only an optical fiber has to be positioned near the sample surface. Therefore, lengthy optical alignments can be avoided. Similarly, its integration ability into a micro-incubator will permit long term living cell observation. Because iSOM can work in various

#139255 - $15.00 USD Received 6 Dec 2010; revised 21 Jan 2011; accepted 23 Jan 2011; published 27 Jan 2011
(C) 2011 OSA

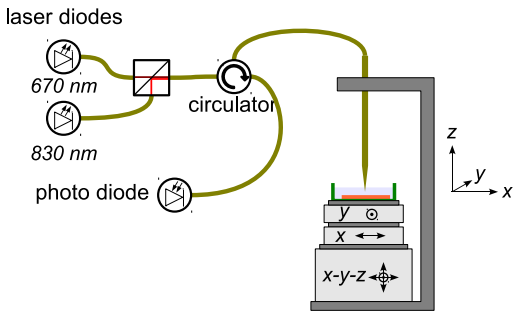

Fig. 1. Schematic view of the iSOM set-up

environments, such as liquids, vacuum, or even low temperatures, we expect it to cover a broad range of applications. Here, we focus on cell imaging in liquid.

2. Experimental

2.1. interferometric Scanning Optical Microscope (iSOM)

The heart of iSOM is the optical fiber tip which is scanned relative to the sample at vertical or axial distances in the order of a few microns. In our set-up the fiber is fixed and the sample is laterally moving (Fig. 1). Two different types of linear translation stages are used for positioning and scanning. Translation stages with piezoelectric inertial motors (Mechonics MS30) with 15 nm resolution and 18 mm range allow for selecting laterally the region to be imaged. For image scanning, a three axis piezoelectric nanopositioning system (Mad City Labs Nano-3D200) is used. Typical images of 200×200 μm^2 with 256×256 pixels can be recorded in about 4 minutes using a speed of 0.5 s/line. The Nano-3D200 is also used for fine tuning the fiber tip height. For the coarse approach the fiber holder is mounted on a manual micrometer translation stage.

The optical part of iSOM mostly uses optical fibers. Thus, no alignment is necessary and the components can easily be changed. Two different laser diodes were used for imaging: a fiber-coupled laser diode emitting at 670 nm (Schäfter & Kirchhoff) and a pigtailed laser diode with 830 nm wavelength (Thorlabs LPS-830-FC/APC). The output of the two laser diodes are combined by a dielectric mirror mounted inside a fiber coupled beam combining unit from Schäfter & Kirchhoff. Thus, the wavelength can be changed without touching the optical set-up. A wide-band polarization insensitive optical circulator (AC photonics PIOC-3-83-P-2-1-1-11) is used to guide the incoming light to the iSOM fiber tip and the reflected intensity to a fiber-coupled amplified photoreceiver (Newfocus 2001-FC). The whole set-up is computer controlled using an available Nanonis SPM controller. A data acquisition computer card with controlling software would, however, be sufficient to run the experiment.

The iSOM probe tip is the key element that determines the quality of the measurements. Their strong divergence prohibits the use of cleaved fibers. Homemade optimized chemically-etched fibers of conical shape [10] with main tip angles of 20° and 30 nm radius of curvature at the apex were used [11, 12]. These fibers allow efficient imaging for fiber sample distances of up to 50 μm.

2.2. Working principle

iSOM exploits the interference of the light reflected at the fiber tip $E_{ir} = r_{ir} \cdot E_0$ with the light reflected from the sample wich is recaptured by the fibre $E_{or} = r_{or} \cdot E_0 = t r_s \gamma \cdot E_0$, with E_0 the

#139255 - $15.00 USD Received 6 Dec 2010; revised 21 Jan 2011; accepted 23 Jan 2011; published 27 Jan 2011
(C) 2011 OSA

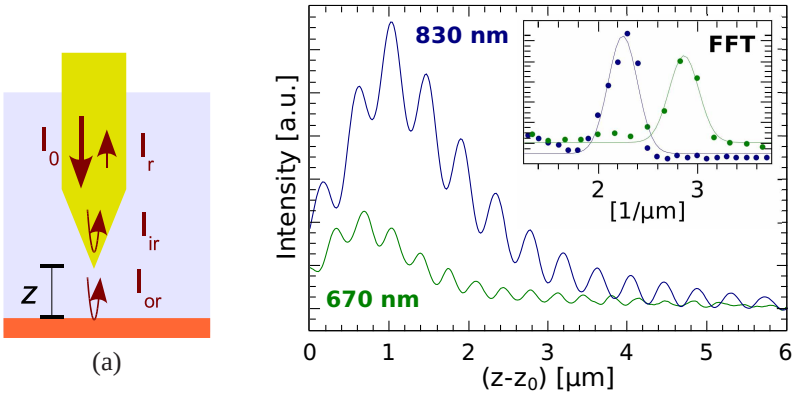

Fig. 2. (a) Scheme of the iSOM working principle. (b) z-scan curves on a bare glass substrate for two wavelengths. The inset shows the FFT.

complex incomming light field amplitude, $r_{ir/or}$ the inner/outer tip reflectivity, t the transmission for fibre outcoupling, $r_s = |r_s|e^{i\phi_s}$ the complex sample reflectivity, and γ the efficiency for light recapturing by the fiber tip. The latter includes all relevant effects, e.g. imperfect vertical fiber alignment. The measured global reflected intensity can be calculated as:

$$I_r(z) = I_{ir} + I_{or} + 2\sqrt{I_{ir}I_{or}}\cos(\phi) = \left[R_{ir} + R_{or} + 2\sqrt{R_{ir}R_{or}}\cos(\phi)\right] \cdot I_0 \qquad (1)$$

with $I_0 = |E_0|^2$ the incident intensity, $R_{ir/or} = |r_{ir/or}|^2$ the inner/ outer reflectance and $\phi = (4\pi/\lambda)z + \phi_s$ the phase shift between E_{ir} and E_{or}. The reflection phase shift (ϕ_s) becomes important for samples with complex transmission/ reflection functions.

The cosine term in Eq. (1) results in interference fringes in the $I_r(z)$ curves, which we call z-scans. The z-scan of a bare glass substrate is shown in Fig. 2(b) for two wavelengths. In this case, the minimal fiber sample distance was estimated at $z_0 \leq 100$ nm. The interference fringes described by Eq. (1). are clearly visible. The measured periods, calculated using Fast Fourier Transformation (FFT, see inset), are 2.87 and 2.25 μm^{-1} for 670 and 830 nm wavelengths, respectively. These values are slightly lower than the nominal values of 2.98 and 2.41 μm^{-1}.

The mean intensity and the visibility of the interference fringes show a maximum at $(z - z_0) \approx 0.7$ and 1.0 μm for $\lambda = 670$ and 830 nm, respectively. At large distances the beam divergence leads to lower back-coupled intensity I_{or}. Consequently, the fringes amplitude decreases and the mean intensity converges to I_{ir}, which is independent of z. The reasons for the intensity decrease at small distance are more complex. In fact, for distances smaller than the wavelength, the optical near-field in the vicinity of the fiber tip becomes more intense and the actual field distribution is more complicated [13, 14, 15, 16]. Thus the description of the reflected intensity I_{or} must be modified. The in-depth treatment in this case is, however, not the scope of the present paper.

The evolution of the interference fringes for distances up to 50 μm was also studied on fixed neurons (Fig. 3). These curves were recorded above and beside one soma on a fixed neuron culture made on silicon substrate and covered with water. The reference distance above the substrate $z_0 > 5$ μm is equal for both curves, but much larger than in Fig. 2. Hence, the intensity maximum observed in Fig. 2 is not visible. The interference fringes remain visible for distances up to 50 μm.

For the z-scan beside the soma, i.e. on a homogeneous surface, one single interference fre-

#139255 - $15.00 USD Received 6 Dec 2010; revised 21 Jan 2011; accepted 23 Jan 2011; published 27 Jan 2011
(C) 2011 OSA

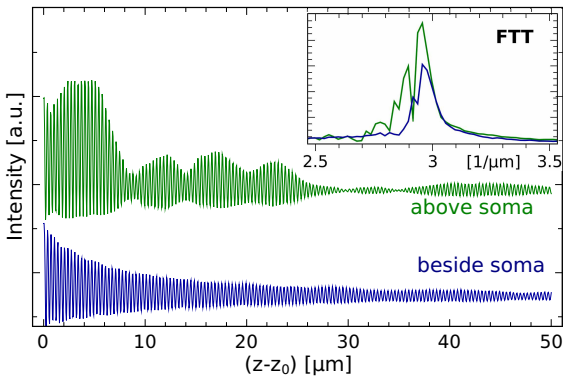

Fig. 3. *z*-scan curves above and beside a neuronal sona in water ($\lambda = 830$ nm). The inset shows the FFT.

quency peak is observed at 2.97 μm^{-1} in the FFT spectra. For the case above the soma, supplementary frequency peaks on the low frequency side of the main peak are observed. The mixing of these interference frequencies results in the observed long range oscillations.

These measurements shows that using an optical fiber tip is very important. Experiments with cleaved fibers showed that their strong light beam divergence inhibits any imaging. In fact a fiber tip can be seen as an axicon, which is well known to generate Bessel beams, well-collimated over large distances exceeding several microns [17, 18]. The fact that we can observe interference fringes for fiber tip - sample distances up to 50 μm shows the quality of our beam. On the other hand, the supplementary frequencies (or interferences) observed on non-homogeneous samples (Fig. 3, green curve) are a hint that some beam divergence remains.

The lateral extension of the Bessel beam is diffraction limited to about half the wavelength. The resolution in the $x-y$ plane is thus of the same order, such as with other far-field imaging techniques. The vertical resolution strongly depends on the interference fringe visibility, i.e. the sample reflectivity. For the $\lambda = 830$ nm measurement as shown in Fig. 2(b), the resolution can be estimated to be better than 20 nm. For highly reflective samples values below 10 nm are feasible.

2.3. Fibroblast

NIH-3T3 fibroblasts are cultivated as described in [19, 20]. In brief, they are cultivated in DMEM complemented with 10% of inactivated fetal calf serum, streptomycin and penicillin. They are harvested at 80% of confluence with trypsin/EDTA and plated on glass substrates coated with fibronectin fragment type III domain 7-10 [21]. Prior to fibronectin coating, glass substrates are covered with a sputtered 1000 Å titanium layer. The titanium layer is patterned using ion milling to yield a numbered grid structure that eases the imaging of the same cells with various techniques.

After the fibronectin coating, the cells are inoculated onto the substrate and spread for several hours. They are fixed by two different methods. In the first experiment PBS with 3% paraformaldehyde supplemented with 2% sucrose was used for 5 min at room temperature. In the second experiment methanol fixation was used by dipping PBS rinsed substrates into cold methanol at -20°C for 10 minutes.

#139255 - $15.00 USD Received 6 Dec 2010; revised 21 Jan 2011; accepted 23 Jan 2011; published 27 Jan 2011
(C) 2011 OSA

2.4. Neurons

Neurons consit of a cell body (or ”soma”) and a burgeoning of fine cables (neurites). Neuronal cultures were prepared as described by Dotti et al. [22]. Briefly, hippocampi brain tissues from E18.5 (embryonic day 18.5) mice were removed and digested in 0.25% trypsin in Hepes-buffered Hanks' balanced salt solution at 37°C for 15 min. After manual dissociation, cells were plated in a concentration of 5,000-15,000 cells/cm^2 in DMEM-10% fetal bovine serum on different substrates. Usual poly-L-lysine (PLL)-coated coverslips lead to uniform cultures with arbitrary cell connections, while patterned surfaces could be used to direct neural growth. In this last case, PLL patterns were transferred on silanized silicon chips [23] using UV classical photolithography steps, including Shipley S1805 photoresist spinning, insulation through a mask, development, PLL deposition (1mg/ml one night) and lift-off in an ultra-sound ethanol bath. One hour after plating, the medium was changed to DMEM containing B27 and N2 supplements. All culture media present a stable pH value of 7.8 under the 5% CO_2 atmosphere provided by commercial incubators regulated at 37°C. Living cells were observed in this work after 21 days of *in vitro* culture (DIV 21) at room temperature and ambient atmosphere. Under these conditions, cell survival is of a few hours.

Cell development can also be stopped by a process called fixation that kept the initial cellular morphology. Neurons were here treated in fixative solutions containing paraformaldehyde (PFA) 4% and HMDS [24] for an optimal shape preservation.

3. Imaging results and discussion

3.1. Fibroblasts

The fixed fibroblasts spread on glass substrates are imaged by iSOM in liquid environment, and by AFM and phase contrast microscopy for comparison (Fig. 4). The iSOM image is built by superposition of about 20 single scans of 40×40 μm^2 size. On iSOM and phase contrast images, three cells of different forms can clearly be distinguished. The two imaging techniques provide complementary information. The phase contrast microscopy image clearly shows the cell outlines and some structures in the cytosol in and around the nucleus.

The iSOM image depicts the cells' topography by contour lines. The distance between each dark/ bright line corresponds to half the wavelength. The upper right cell shows 11 lines from its border to the center. The corresponding height of 3.7 μm is in good agreement with this kind of cell. As the reflection on the cell surface is not total, the iSOM image contains more information than solely the position of the interface. In the figure, this is better seen for the lower left hand cell. Its inner structure is revealed by dark spots. With models yet to be developed it will be possible to get more information on the nature of the material inside the cell volume.

The AFM image shows the lower cell visible in Fig. 4(a) and (b) and zoomed in Fig. 4(d). Similar to the iSOM image the AFM one is built from about 10 single scans. The cell shape with its ramifications is clearly visible and the cell nucleus contours are revealed. Compared to the iSOM image the AFM one shows more details at the border of the cell. The higher resolution of the AFM image is at the cost of longer acquisition time. Although the cell imaged by AFM was dried by blowing clean air, its height as measured by AFM qualitatively matches the height measured by iSOM showing no qualitative volume change upon drying.

In order to check the interpretation of the lines as contour lines in the iSOM image, we have made the same measurements on a similar cell, but making use of two different wavelengths. The corresponding topographies were calculated for a cross section as shown on Fig. 5. A very good agreement is obtained. As expected, the comparison of the two iSOM images shows a slightly better resolution at smaller imaging wavelength.

#139255 - $15.00 USD Received 6 Dec 2010; revised 21 Jan 2011; accepted 23 Jan 2011; published 27 Jan 2011
(C) 2011 OSA

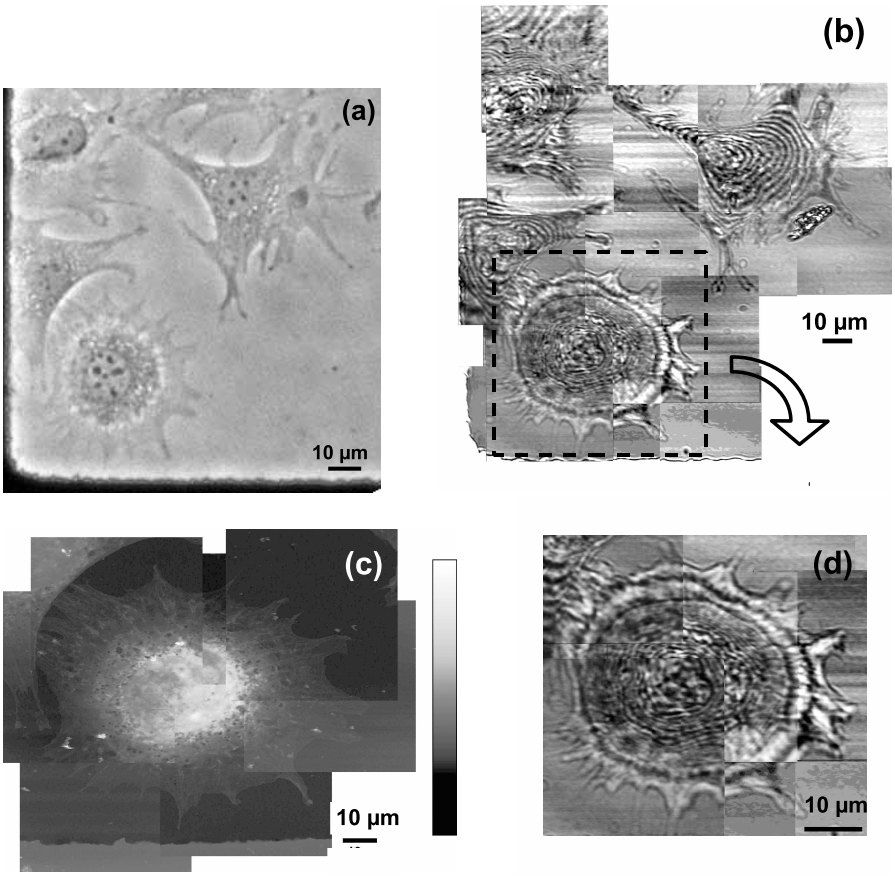

Fig. 4. Fixed fibroblast cells observed by (a) phase-contrast microscopy, (b,d) iSOM, and (c) AFM. (c) and (b) show the lower left cell visible in (a) and (b). The span of the color bar in (c) corresponds to 760 nm. The distribution of the greyscale corresponds to a linear distribution modified by a gamma value of 0.65 to enhance the contrast.

3.2. Neurons

Neurons grown on two kinds of substrates, silicon chips (Fig. 6) and coverslips (Fig. 7), have been observed. The silicon chips are used to investigate the local electric activity of neurons grown on their surface. In order to locate specific neurite positions right above the silicon sensors, cell growth was guided along to specific geometries [25].

The SEM and iSOM images of the same neuron fixed after 3 days of culture on a silicon chip is shown on Fig. 6. The neuron's soma and neurites can clearly be distinguished on the metallic lines. Some details have been changed between the two images. In the SEM image, the neurite leaving on the lower right part of the soma is suspended over the edge of the metal strip. In the iSOM image this same neurite is broken. Moreover the smaller soma visible on the left side of the SEM image has disappeared on the iSOM image. Even if the SEM image is somehow more precise, the iSOM image clearly reveals the main features and gives a good three dimensional impression. The topography of the soma is visible as interference fringes.

Compared to SEM, one important advantage of iSOM is the possibility to image living cells. The use of pH-buffered solutions already allowed to keep neurons alive for about three hours, but an improvement of life conditions could be easily implemented around the fibered micro-

#139255 - $15.00 USD Received 6 Dec 2010; revised 21 Jan 2011; accepted 23 Jan 2011; published 27 Jan 2011
(C) 2011 OSA

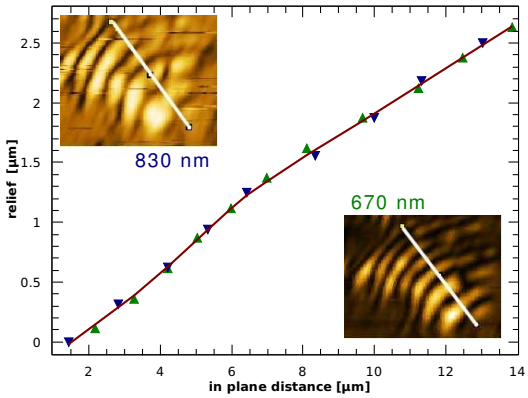

Fig. 5. Calculation of the cell topography from iSOM measurements made at two wavelengths. The white lines indicate the chosen cross section.

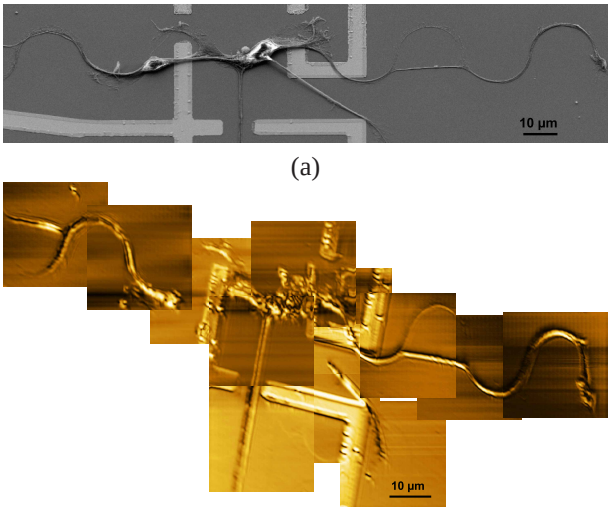

(a)

(b)

Fig. 6. Fixed neurons on an electronic substrate observed by (a) SEM and (b) iSOM.

scope. Compared to phase contrast microscopy, iSOM allows informative 2 1/2D images to be obtained. For example, as visualized on ”old” cultures where the different neurons form mature connections, neurites of the finest diameters appear smooth unlike the thicker ones (Fig. 7). Such information on living neurons are biologically pertinent.

The iSOM image gives a clear impression of the topography and many details are revealed. However, no fringes are visible, even for nominal cell heights of some microns. In fact, the refractive index difference between the solution and the cell is too small to ensure efficient reflection at the cell surface. The light is thus penetrating the cell and reflected by the substrate. The observed image is due to the phase shift encountered during the propagation inside the cell (ϕ in Eq. (1))

#139255 - $15.00 USD Received 6 Dec 2010; revised 21 Jan 2011; accepted 23 Jan 2011; published 27 Jan 2011
(C) 2011 OSA

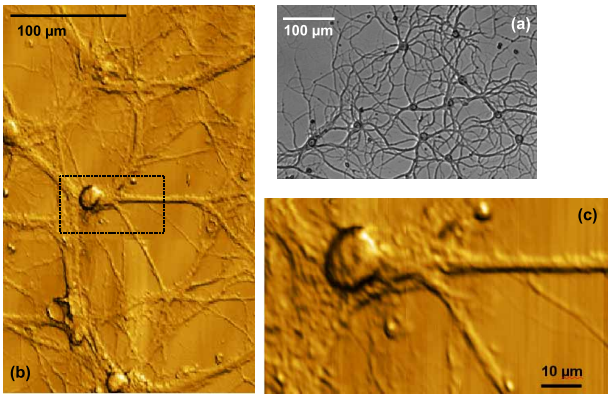

Fig. 7. Living neurons observed by (a) phase contrast microscopy and (b-c) iSOM.

4. Conclusion

We have presented the ability of iSOM for imaging different biological cells including living neurons in liquid. The obtained images reveal many details and render a clear perception of the cells' topography. Furthermore, iSOM minimizes the impact on the cells, as it is a contactless minimally invasive method. In addition, iSOM can also operate in aqueous environments. Because the microscope head is very compact and requires only a small free space to be available around the sample, it can easily be integrated into existing systems. For instance, its impact on living cells could be further minimized by the implementation of a mini-incubator for temperature and pH control. Under such circumstances, we expect iSOM to be able to track living cells for hours, allowing for example the study of mechanical deformation associated with either growth or electrical activity of neurons [26].

Acknowledgments

We thank the Thermometry and Calorimetry team and J.F. Motte from Institut Néel for the fibroblast substrate preparation and fiber tip fabrication, respectively.

#139255 - $15.00 USD Received 6 Dec 2010; revised 21 Jan 2011; accepted 23 Jan 2011; published 27 Jan 2011
(C) 2011 OSA